IEEE Access
Multidisciplinary | Rapid Review | Open Access Journal

Received October 13, 2021, accepted October 23, 2021, date of publication October 27, 2021, date of current version November 4, 2021.

Digital Object Identifier 10.1109/ACCESS.2021.3123366

Wideband Flexible/Transparent Connected-Ground MIMO Antennas for Sub-6 GHz 5G and WLAN Applications

ARPAN DESAI[1,2], (Senior Member, IEEE), MERIH PALANDOKEN[3], (Senior Member, IEEE), JAYSHRI KULKARNI[4], (Member, IEEE), GANGIL BYUN[5], (Senior Member, IEEE), AND TRUONG KHANG NGUYEN[1,6], (Member, IEEE)

[1]Division of Computational Physics, Institute for Computational Science, Ton Duc Thang University, Ho Chi Minh City 758307, Vietnam
[2]Department of Electronics and Communication Engineering, CSPIT, Charotar University of Science and Technology (CHARUSAT), Changa 388421, India
[3]Department of Electrical and Electronics Engineering, Izmir Katip Celebi University, 35620 Izmir, Turkey
[4]Department of Electronics and Telecommunication Engineering, Vishwakarma Institute of Information Technology, Pune 411048, India
[5]School of Electrical Engineering, Ulsan National Institute of Science and Technology (UNIST), Ulsan 44919, South Korea
[6]Faculty of Electrical and Electronics Engineering, Ton Duc Thang University, Ho Chi Minh City 758307, Vietnam

Corresponding author: Truong Khang Nguyen (nguyentruongkhang@tdtu.edu.vn)

This work was supported by the National Research Foundation of Korea (NRF) funded by the Government of Korea (MSIT) under Grant NRF-2021R1C1C1012955.

ABSTRACT A flexible transparent wideband four-element MIMO antenna with a connected ground plane is proposed with numerical computation and experimental measurement studies. The optical transparency is obtained using flexible conductive oxide material AgHT-4 and Melinex substrate. The radiating elements are in the form of circular stub-loaded C-shaped resonators, which are positioned in a carefully structured flexible Melinex substrate with an interconnected partial ground plane structured in the form of an L-shaped resonator, attaining an overall antenna size of $0.33\lambda \times 0.48\lambda$ at the lowest operating frequency. The proposed antenna spans over a -10 dB impedance bandwidth of 2.21-6 GHz (92.32%) with an isolation level greater than 15dB among all elements. The maximum gain is 0.53dBi with a minimum efficiency of 41%, respectively which is satisfactory considering flexible structure and sheet impedance of 4Ω/sq. MIMO antenna parameters in terms of the envelope correlation coefficient (ECC) and diversity gain (DG) are also extracted where all the values are satisfactory for MIMO applications. The bending analysis of the proposed transparent MIMO antenna along the X and Y axis has revealed good performance in terms of scattering parameters and radiation pattern along with MIMO diversity performance. All of these technical points make the flexible MIMO antenna suitable for smart devices using sub-6 GHz 5G and WLAN band in IoT applications where visual clutter and co-site location issues need to be mitigated with the integration ease of conformal placement on the curved component/device surfaces.

INDEX TERMS Flexible, MIMO, sub 6 GHz 5G, transparent, wideband, WLAN.

I. INTRODUCTION

The emergence of 5G that provides minimal latency and allows a larger volume of data transfer has become one of the backbones for wireless communications [1]. The conventional antenna designs have to be upgraded for this advanced technology. As wireless devices become more condensed, the technical requirement for novel antennas with compact structure, wider bandwidth, and satisfactory gain is in great demand. Transparent antennas, which enable engineers to innovate the current designs for IoT applications that unobtrusively blend into architectural fixtures like windows, glazed artwork, or overhead lights, are currently being explored. The optical transparency allows more antennas to be installed near the points of usage to increase the signal strength and data speeds [2]. This type of antennas is typically realized using conductive oxides or conductive inks which can be printed on the transparent substrate [3], [4].

For sub-6 GHz 5G infrastructure, the enhancement of spectral efficiency and channel capacities requires MIMO

The associate editor coordinating the review of this manuscript and approving it for publication was Sotirios Goudos.

antenna systems with wide bandwidth [5], [6]. Numerous non-transparent wideband MIMO antennas have been proposed using different structures such as L-shaped slot [7], inverted-F patch geometry [8], monopole [9], inverted L-shaped monopole [10], inverted L-shaped monopole with SRR [11], the circular metallic disc [12], integrated balun with dipole [13], and square rings coupled through proximity feed [14]. All of these have been designed with a connected ground as a requirement for a MIMO system [15]. It is noted that MIMO systems with split ground planes [16], [17] may provide higher isolation but are impractical for real application.

Most of the aforementioned designs are challenging to adapt to a transparent structure because those isolation enhancement techniques such as using vias and decoupling structures are not preferred to maintain transparency and to keep a low-cost manufacturing process. A few transparent MIMO antennas have been proposed for dual-band and wide-band applications using 2-element [18]–[20] or 4-element structures [21]. The transparent antenna design in [18] achieved good DG and ECC with the technical drawback of operation with a separate ground plane. The isolation levels were also not mentioned and the overall antenna size is large. Antenna in [19] achieves good transparency with dual-band operation however the efficiency is lower than 40% and no MIMO parameters are analyzed. A transparent antenna in [20] is fabricated for a single element only and no MIMO analysis is carried out. The antenna design in [21] shows wideband performance with good diversity performance however it is proposed for mm-wave application with relatively large size.

Flexible antennas proposed in [23]–[28] are non-transparent where the antennas in [24]–[26] have a thickness larger than 1mm, which leads to low flexibility. Also, the antennas in [22]–[25], [28] are 2 port MIMO configurations which are not desirable for accommodating a much greater number of users. Antennas in [22], [29] are transparent and flexible where [29] has superior performance with 4 elements due to the use of highly conductive NI metallic mesh grown using the electro-deposition technique. However, it is not covering the desired sub-6 GHz band whereas [22] covers the desired band but it uses a thick substrate with only 2 elements of MIMO configuration. The reason for superior performance in [29] is due to the higher conductivity of nanostructured Ni metallic mesh having conductivity exceeding 2×10^6s/m as compared to AgHT-4 which has a conductivity of 1412 s/m.

In this paper, a flexible transparent wideband 4-element MIMO antenna is proposed for sub-6 GHz 5G applications. The parametric studies on the antenna resonator geometry are carried out to obtain the final antenna model with the aim of fabrication errors to be kept possibly small while the isolation level is still high across the wide operation bandwidth. The same is achieved by carefully designing the connected ground plane lines and introducing the slots in the substrate. MIMO antenna parameters are calculated in terms of ECC, and DG, where all the numerically computed and experimentally measured results are satisfying the ideal values, stated in the operation standards under normal and bent conditions along two axes as suggested in [30]–[32].

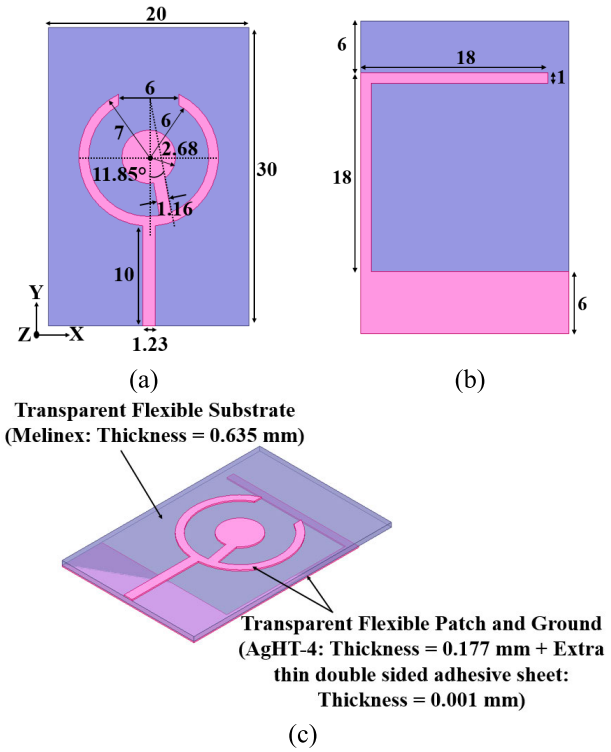

FIGURE 1. Flexible antenna geometry (a)Top view (b) Back view (c) Perspective view (All dimensions are in mm).

II. ANTENNA GEOMETRY

Fig. 1 depicts the geometrical model of a single element transparent radiator simulated using FEM-based ANSYS HFSS software. The antenna element consists of a solid cylindrical-shaped conductive radiator in the form of a C-shaped resonator encompassed in a slotted cylinder which is connected through a tilted horizontal line as a circular stub.

Transparent flexible conductive material AgHT-4 (sheet resistance = 4 Ω/sq, conductivity = 1412 S/m, thickness = 0.177 mm, optical transparency of about 70%) is used to design the conductive patch and partial ground plane. The flexible transparent substrate is in the form of Melinex (dielectric constant (ε_r) = 2.9, loss tangent (tanδ) = 0.06, thickness = 0.635 mm, the optical transparency of about 81%), which are coalesced to form the single element resonator. RF performance analysis in terms of the reflection coefficient is carried out by varying various antenna geometric parameters to justify the chosen resonator geometry as shown in Fig. 2 and Fig. 3.

The inner solid circular radius (R_3) is varied as shown in Fig. 2(a) where it is observed that the reflection coefficient between the frequency band spanning from 2.9 GHz – 3.5 GHz increases with the larger radius however the reflection coefficient at a frequency higher than 3.5 GHz is

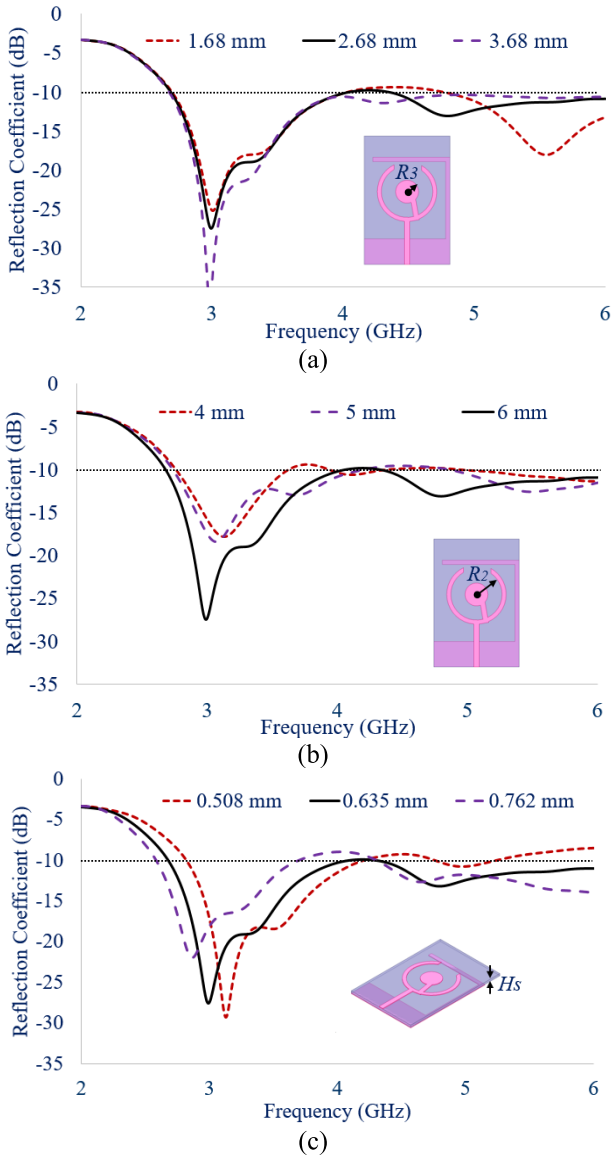

FIGURE 2. Parametric variation of single antenna element (a) Inner solid circular radius (R_3) (b) Outer slotted hollow circular inner radius (R_2) (c) Substrate thickness (H_s).

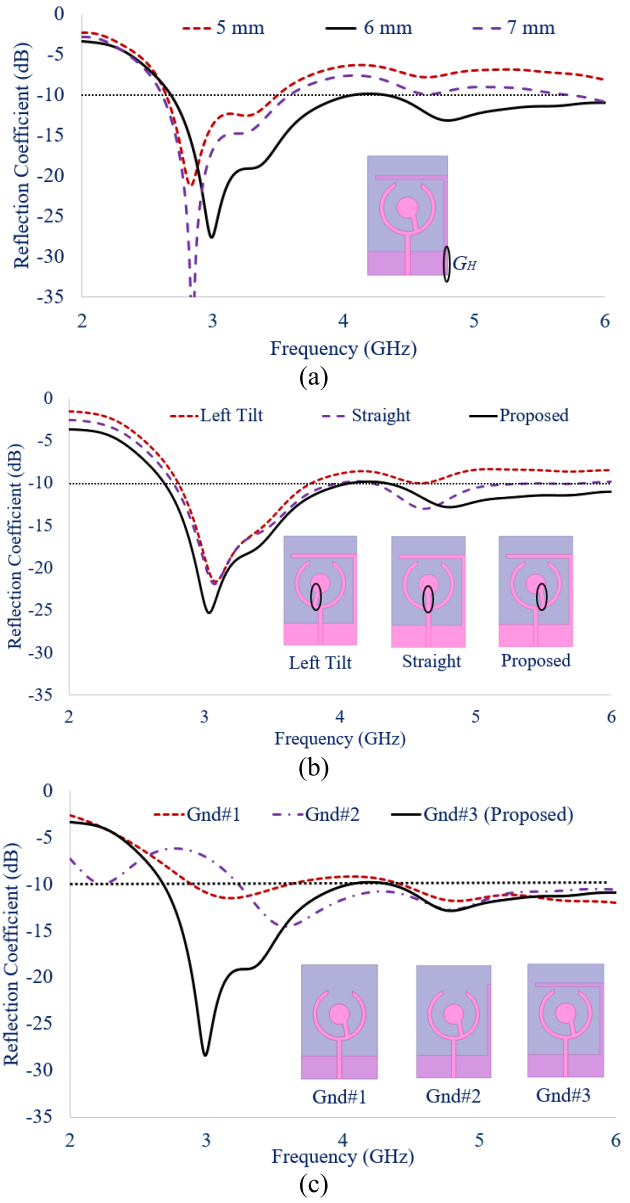

FIGURE 3. Parametric variation of single antenna element (a) Partial ground plane length (G_H) (b) stub position (c) Ground plane evolution.

almost near to -10 dB. The optimum value of R_3 is selected as 2.68 mm which covers the required frequency bands. Fig. 2(b) illustrates that the maximum value of the reflection coefficient and broader impedance bandwidth is achieved when the value of R_2 is chosen as 6 mm. As seen in Fig. 2(c) when the substrate height is increased, the resonance frequency shifts towards the lower value while the minimum effect is observed in terms of impedance bandwidth for two *Hs* values of 0.508 and 0.635 mm, respectively. *Hs* value of 0.762 mm leads to the emergence of a notch band spanning from 3.5 – 4.5 GHz. The *Hs* value is chosen to be 0.635 mm considering the best RF performance.

Numerical analysis in terms of partial ground plane length variation in correspondence to ground plane evolution is illustrated in Fig. 3 (a-b). In Fig. 3 (a), it can be observed that partial ground length (G_H) variation affects the reflection coefficient levels and impedance bandwidth throughout the whole operation band where a G_H value of 6 mm is selected to achieve the targeted operation band. The stub position is also evaluated as shown in Fig. 3(b), where it is depicted that the proposed stub position gives the best results in terms of reflection coefficient levels and bandwidth. The evolution steps of ground plane geometry are presented in Fig. 3(c). The addition of vertical and horizontal lines in the form of an L-shaped resonator over the partial ground plane results in the required bandwidth and reflection coefficient to be achieved.

The optimized single-element antenna is fabricated to carry out the experimental study where the front view is illustrated in Fig. 4. The reflection coefficient of a single element

FIGURE 4. Fabricated prototype of single element flexible antenna.

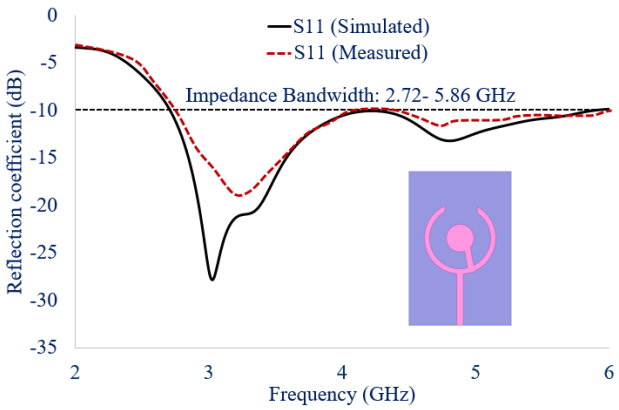

FIGURE 5. Single antenna element and its reflection coefficient.

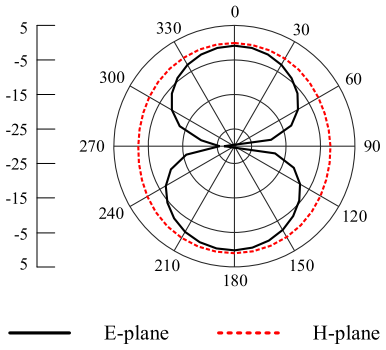

FIGURE 6. 2D Radiation Pattern of Single element antenna.

flexible transparent antenna is measured with Keysight VNA 9912A. The measured S11 parameter is shown in Fig. 5 with the consequence of −10 dB impedance bandwidth between 2.72 GHz and 5.86 GHz with 73.2% percentage bandwidth that agrees well with the numerical computation results.

The 2D radiation pattern of single element flexible antenna is illustrated in Fig. 6 where dipole and the omnidirectional shaped pattern is achieved along with E and H plane, respectively.

To model the flexible transparent 4-element MIMO antenna, each of four elements is arranged as shown in Fig. 7. The lower mutual coupling among the elements with the

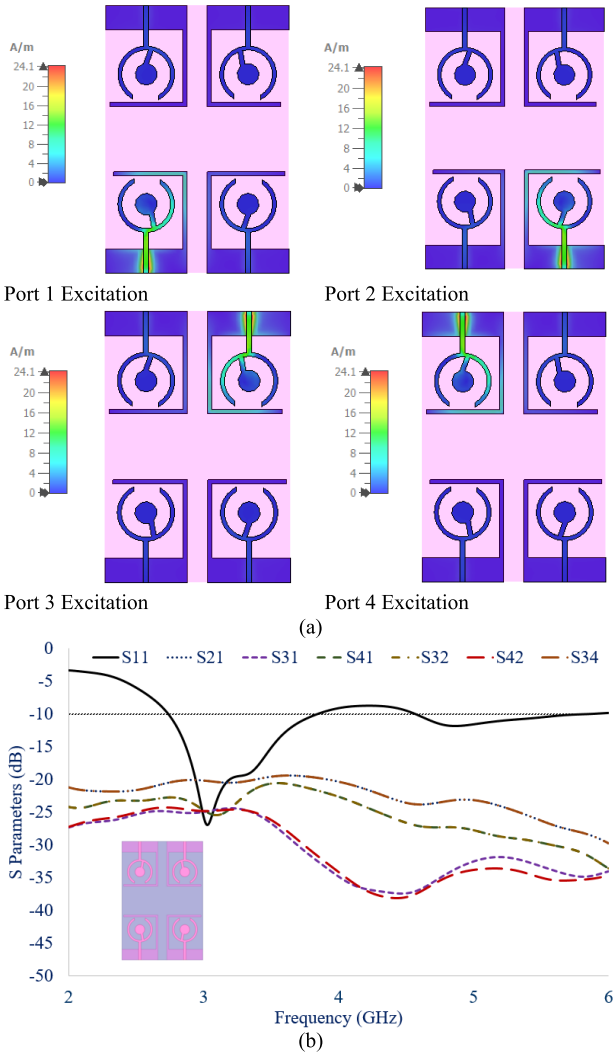

FIGURE 7. Ground plane selection (Case 1) (a) Current Distribution at 3 GHz (b) S-Parameters.

connected ground plane [15] is needed to substantiate the correct interpretation of signal levels in real-time systems. To achieve a low mutual coupling level with a common ground plane is not a trivial task since it leads to significant coupling as the resonant surface current can flow along the connecting path among each antenna element. To investigate this issue, the surface currents are plotted in step-wise optimization by exciting the antenna element at Port 1 for three different cases at the respective resonance frequency as shown in Fig. 7 and Fig. 8 followed by which the common ground design is derived as shown in Fig. 9.

Case 1 illustrates the geometrical arrangement of 4 antenna elements in a mirrored symmetrical form with separate ground planes as shown in Fig. 7. As the ground planes are separate, the negligible amount of excited surface current is coupled with the adjacent elements as illustrated in Fig. 7(a) that leads to high isolation level greater than 20dB. However, the notch band is observed between 3.5- 4.5 GHz as observed in Fig. 7(b).

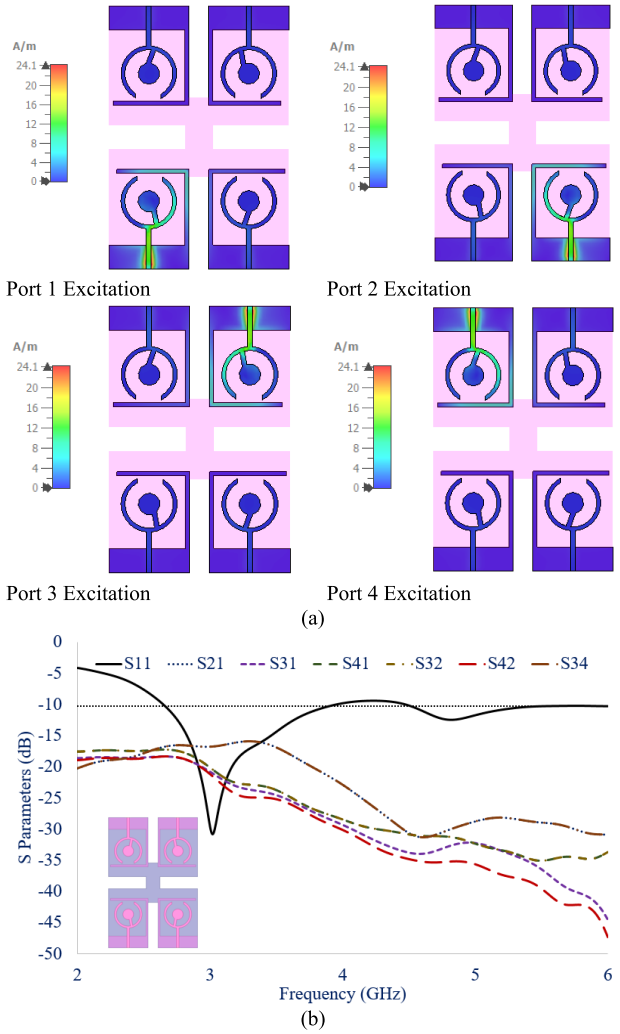

FIGURE 8. **Ground plane selection (Case 2) (a) Current Distribution at 3 GHz (b) S-Parameters.**

Case 2 illustrates the second step where the ground planes of each antenna element are still separated while the rectangular slots are introduced in the substrate as shown in Fig. 8. As deduced from Fig. 8, having the rectangular slots in the substrate not only makes the MIMO antenna more flexible but also helps to maintain the required isolation levels greater than 15dB. The surface current distributions at the resonance frequencies are plotted where it is observed that significant improvement in terms of isolation level is achieved at higher bands while the isolation level is still greater than 15 dB at lower bands. However, the antenna design has still separated ground planes, thus, a further design modification is needed.

The previous two cases show that it is important to modify the substrate to achieve more flexibility while achieving the isolation levels greater than 15dB over the desired bandwidth for an optimal MIMO performance. The common ground plane has to be achieved for which further geometric modification in the ground plane is carried out in Case 3 as shown in Fig. 9. A rectangular-shaped conductive oxide material is added on the bottom side of the substrate into the middle part to connect all the ground planes of 4 element MIMO thus designing a connected ground antenna system. To illustrate the resulting RF performance, the surface current distributions at 3 GHz for the excitation of ports 1-4 are plotted in Fig. 9(a). It is observed that a negligible amount of excited resonant current is coupled to the other three ground locations, which leads to a high inter-element isolation level

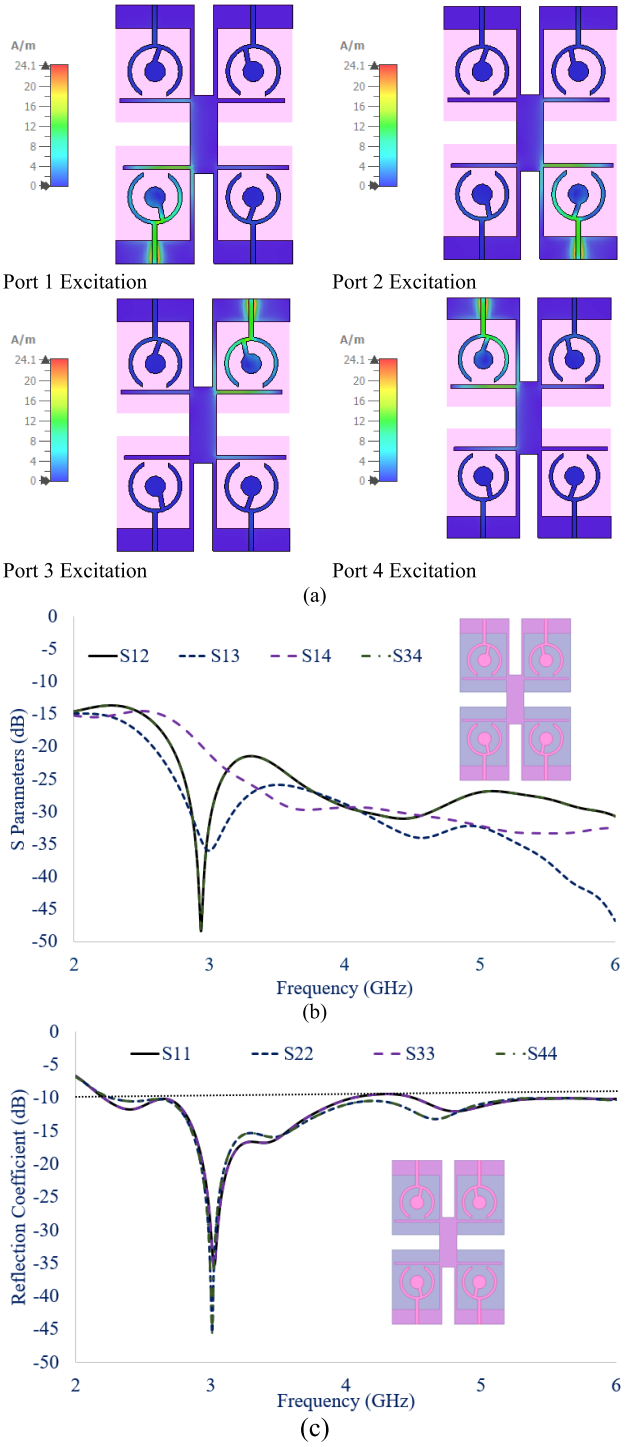

FIGURE 9. **Proposed ground plane (Case 3) (a) Current distribution at 3 GHz (b) Isolation levels (c) |S11|.**

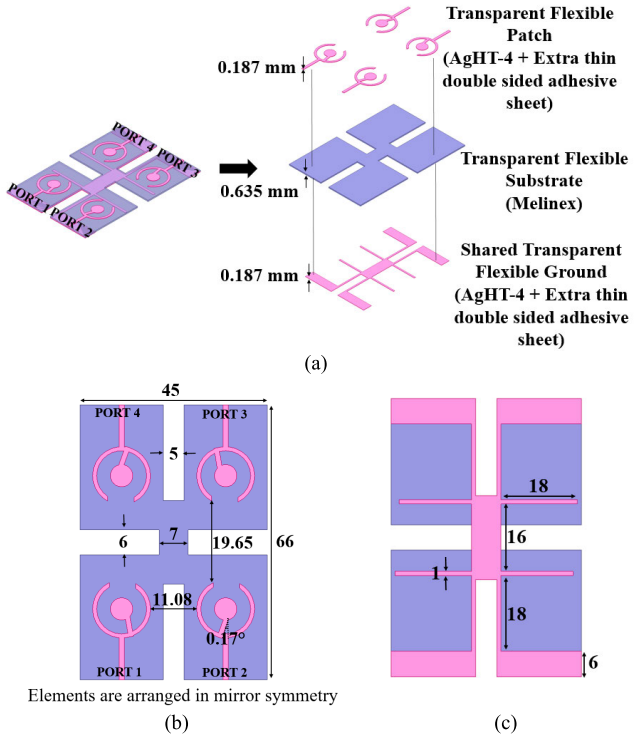

FIGURE 10. Antenna geometry of 4 elements MIMO (a) Layered view (b)Top view (c) Back view (All dimensions are in mm).

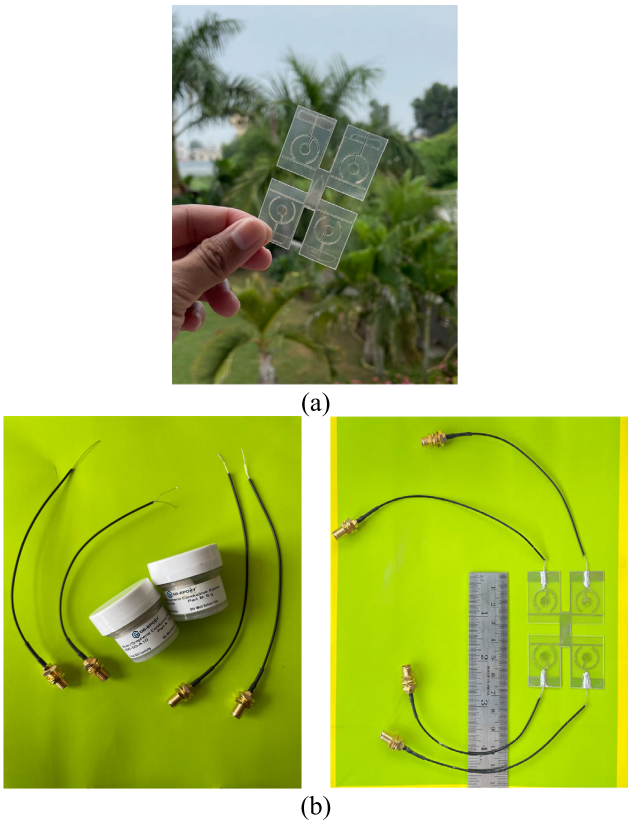

FIGURE 11. Fabricated 4 elements transparent MIMO antenna (a) Front view (b) Antenna with feeding cable and conductive adhesive.

greater than 15dB as shown in Fig. 9(b). This points out the positive effect of selected shared ground structures on the reduction of the surface currents traversing in other ground locations. Wideband characteristics with a good reflection coefficient performance are shown in Fig. 9(c) where the simulated impedance bandwidth extends from 2.21GHz to 6 GHz with 92.32% percentage bandwidth covering the sub-6 GHz and WLAN bands.

In summary, a high isolation level greater than 15dB across wide bandwidth is achieved with a practically manufacturable structure while achieving the required flexibility in addition to system transparency. The proposed flexible MIMO antenna design avoids alternative complex mechanisms including the introduction of vias and decoupling structures, which is almost impossible to implement in a transparent antenna design.

The final version of the flexible transparent MIMO antenna is shown in Fig. 10 along with the fabricated prototype in Fig. 11. The extra thin double-sided adhesive tape with the thickness of 0.01mm is utilized to interface the AgHT-4 sheet on top and bottom sides of the transparent flexible Melinex substrate forming a completely transparent device. The four ports on the top side of the MIMO antenna are fed through SMA Female to UFL connector whereas only a single connection is done on the bottom side due to the connected ground plane. The conductive adhesive made up of Silver and Graphene is used for the connector sticking to avoid the hot solder process which may affect the conductivity value of the silver oxide sheet.

III. RESULTS AND DISCUSSION

To illustrate the positive effect of the connected ground plane, the S-parameters of the proposed flexible transparent 4-element MIMO system are illustrated in Fig. 12(a-b). The vertical and horizontal distances separating each antenna element are 19.65 mm and 11.08 mm, which is about 0.148 λ and 0.083 λ at the lowest operating frequency of 2.26 GHz, respectively. It is expected that a connected ground plane should yield a lower isolation level due to the coupling path. Nevertheless, Fig. 12(a) shows that the connected ground structure still exhibits an isolation level greater than 15dB across the wide bandwidth with another advantage of larger impedance bandwidth. High isolation greater than 20dB among all elements is also achieved for the operation frequencies higher than 3 GHz.

The resonance dip within the impedance bandwidth is observed at 3 GHz, which displays the decent agreement while measuring S-parameters with Keysight VNA 9912A as illustrated in Fig. 12 (b). The slight difference in the impedance bandwidth is due to the fabrication mismatch as the conductive oxide (AgHT-4) is patterned with the help of a goldsmith instead of a laser cutter to avoid heat exposure which may alter the conductivity of the sheet and calibration errors. In addition, the use of four SMA female to UFL connectors may add some losses and imperfect contact impedance.

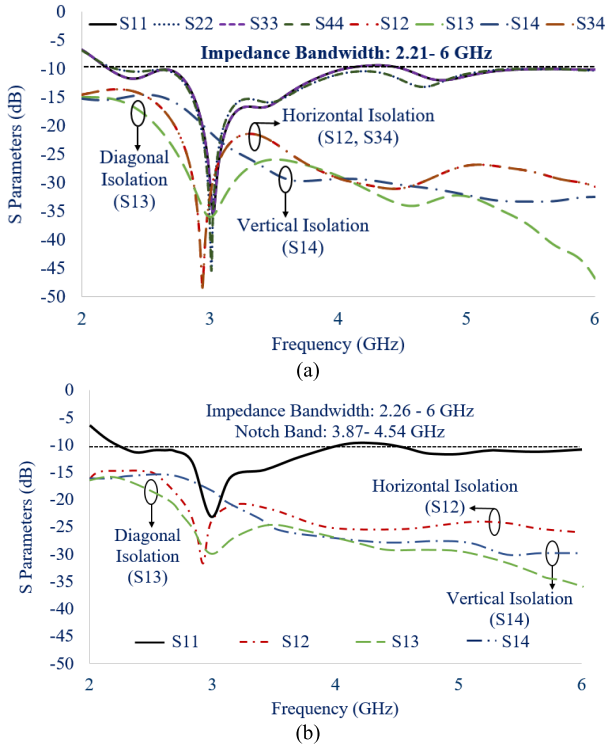

FIGURE 12. S parameters (dB) of 4 elements transparent MIMO antenna with connected ground (a) Simulated (b) Measured.

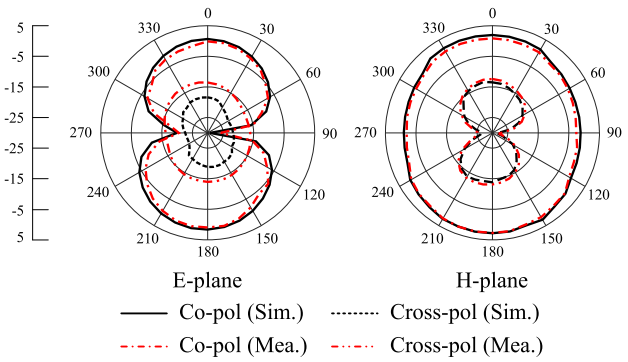

FIGURE 13. Simulated and measured 2D radiation patterns for the proposed antenna at 3 GHz.

The simulated and measured 2-dimensional co/cross-polarization patterns are illustrated in Fig. 13 at XZ (phi = 0) and YZ (phi = 90) planes, respectively, where an isolation level greater than 15dB is observed between co and cross-pol patterns.

One of the important MIMO diversity parameters is ECC which conveys the total amount of correlation between radiated fields among antenna elements in the MIMO antenna system. This parameter gives an idea about the influence of radiation patterns emitted by each element when all the ports are excited simultaneously. Fig 14 (a) illustrates the simulated ECC curves for ports 1,2,3,4 under non-bend conditions. It is observed that the ECC is well below the level of 0.1 for the band of interest except for ECC14, where at the frequency

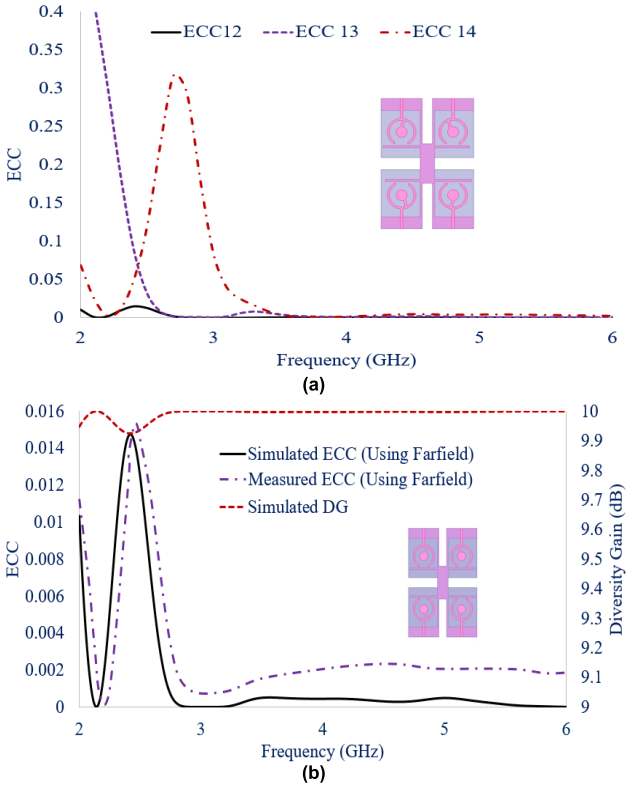

FIGURE 14. (a) Simulated Frequency-variation of Envelope Correlation Coefficient (ECC) (b) ECC12 and Diversity Gain (DG).

band below 3.2 GHz, the ECC > 0.1 due to the degradation in the isolation level resulting from the increased inter-element proximity. Fig. 14 (b) shows the ECC value calculated using a 3D polar plot referring to [33] for the proposed transparent MIMO antenna which is smaller than 0.016 and is well under the limit of 0.1.

The ECC of any two antenna elements of N element MIMO antenna is estimated by using the below equation and graphically illustrated in Fig. 14 [33].

$$\rho_c(i,j,N) = \frac{\iint \left[\mathbf{F}_i(\theta,\phi)\cdot\mathbf{F}_j(\theta,\phi)\right] d(\theta,\phi)}{\sqrt{\iint |\mathbf{F}_i(\theta,\phi)|^2\, d(\theta,\phi)\iint \left|\mathbf{F}_j(\theta,\phi)\right|^2 d(\theta,\phi)}}, \quad (1)$$

where, Fi(O, Ø) and Fj(O, Ø) are the complex radiation patterns of the antennas i and j, respectively when all other antennas are terminated by matched loads (typically 50 Ω). The operator · is the Hermitian product.

The ECC 12 is measured as shown in Fig 14 (b) where it is observed that the numerically computed and experimentally measured results of ECC 12 agree well due to which the other MIMO system parameters including measured ECC 13 and ECC 14 are not shown for the brevity of data.

Diversity gain in the multiple antenna structures points out the enhancement in the signal-to-noise ratio (SNR) compared to SNR level in a single antenna structure. The ideal value of DG should be 10. Fig.14 (b) illustrates the value of DG for the

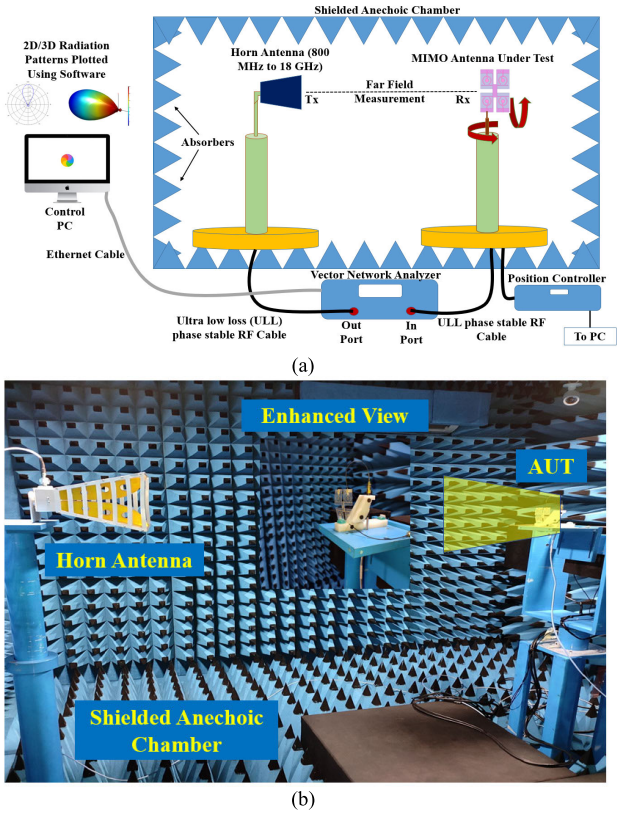

FIGURE 15. Far-Field Measurement Setup (a) Block diagram of the setup (b) Inside the anechoic chamber.

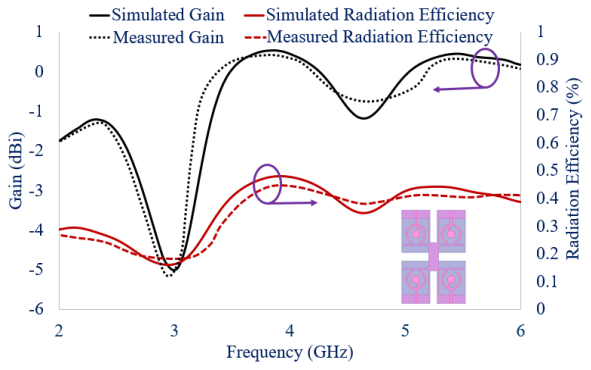

FIGURE 16. Gain and Efficiency of flexible MIMO antenna.

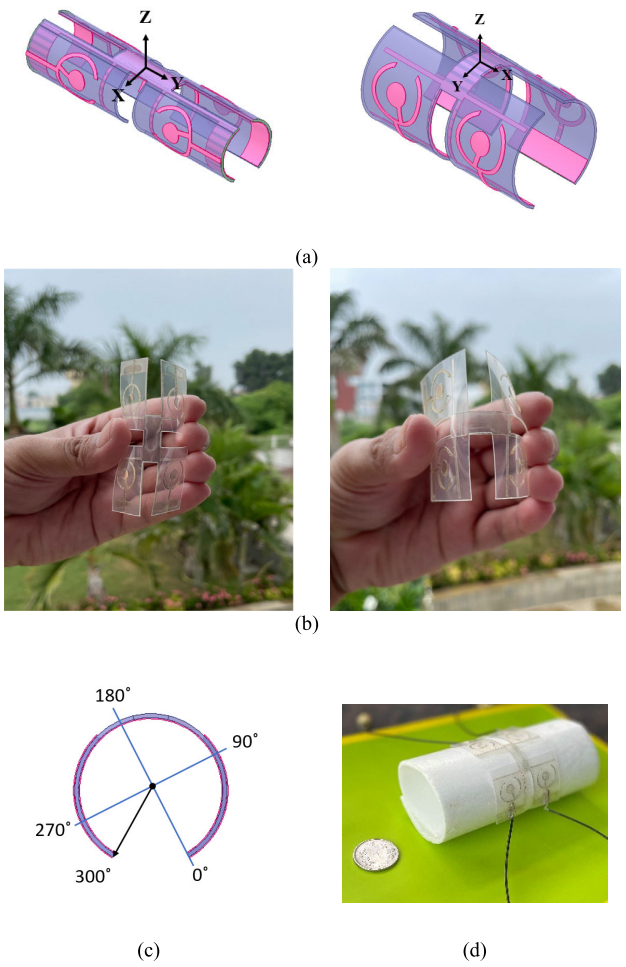

FIGURE 17. Fabricated flexible antenna geometry of 4 elements MIMO antenna (a) Isometric view of bending along X and Y-axis (b) Fabricated view of bending along X and Y-Axis (c) Bending angle illustration (d) Bending over Styrofoam.

proposed transparent MIMO antenna system to be between 9.9-10dB, which is quite well. ECC and DG meet the MIMO diversity criteria where a uniform outdoor propagation environment is considered.

The block diagram of the far-field measurement setup and actual setup inside an anechoic chamber is shown in Fig. 15 (a, b). The peak gain is measured in an anechoic chamber where a 3D radiation pattern can be conveniently obtained for the preset RF input power by measuring the received power level at the receiving antenna side. The numerical integration of radiated power level to be measured by the receiving antenna is done for the calculation of the total radiated power level. The total efficiency can be obtained by dividing the total radiated power by the input power level for the entire band of interest as shown in Fig. 15 with the result of maximum gain as 0.53 dBi while the average radiation efficiency is 41%. It is observed from Fig 16. that the gain and efficiency values are low in comparison to the conventional nonflexible Copper-based antenna designs which are directly dependent on the sheet impedance of the conductive oxide (4 Ω/Sq). While the transparency and conductivity are inversely proportional, the conductivity is lower for the higher optical transparency to be achieved. The low value of conductivity is the main reason for the low efficiency of the transparent MIMO antenna in addition to the high loss tangent of Melinex. The higher thickness ratio between the AgHT-4 and Melinex sheets results in lower radiation efficiency with more power loss in the lossy non-radiating layers. The connector losses using of SMA to UFL connector are the additional factors. However, the gain and efficiency values achieved are quite satisfactory for flexible, transparent, and low conductivity material-based antennas in the literature.

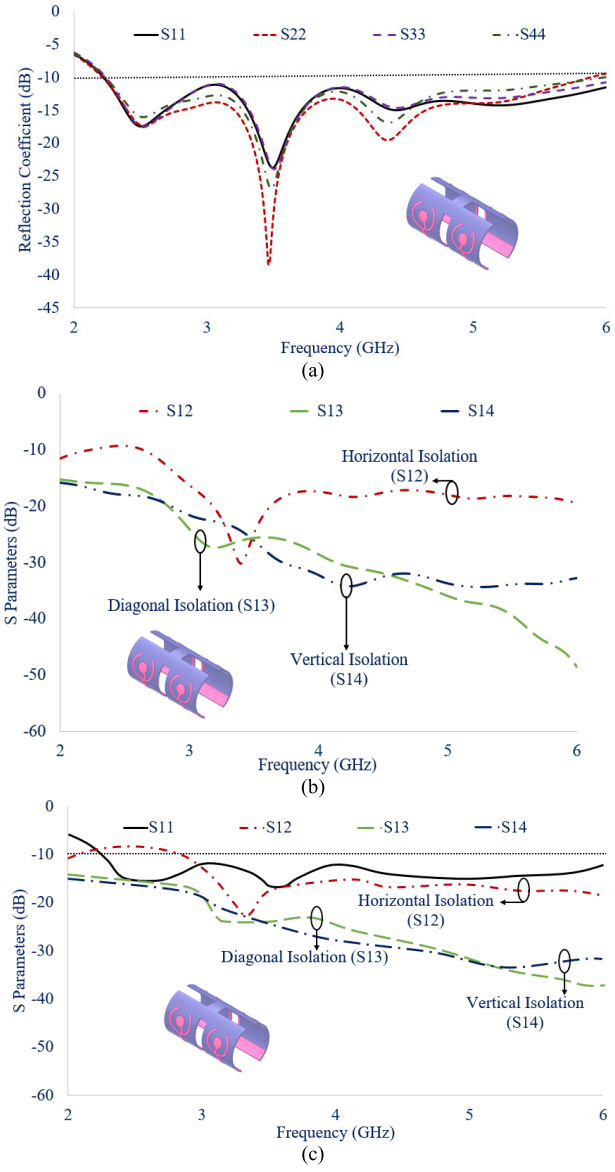

FIGURE 18. Measured S parameters of 4 elements flexible MIMO antenna for bending along Y-axis (a) Scattering parameters (b) Transmission parameters (c) Measured S-parameters.

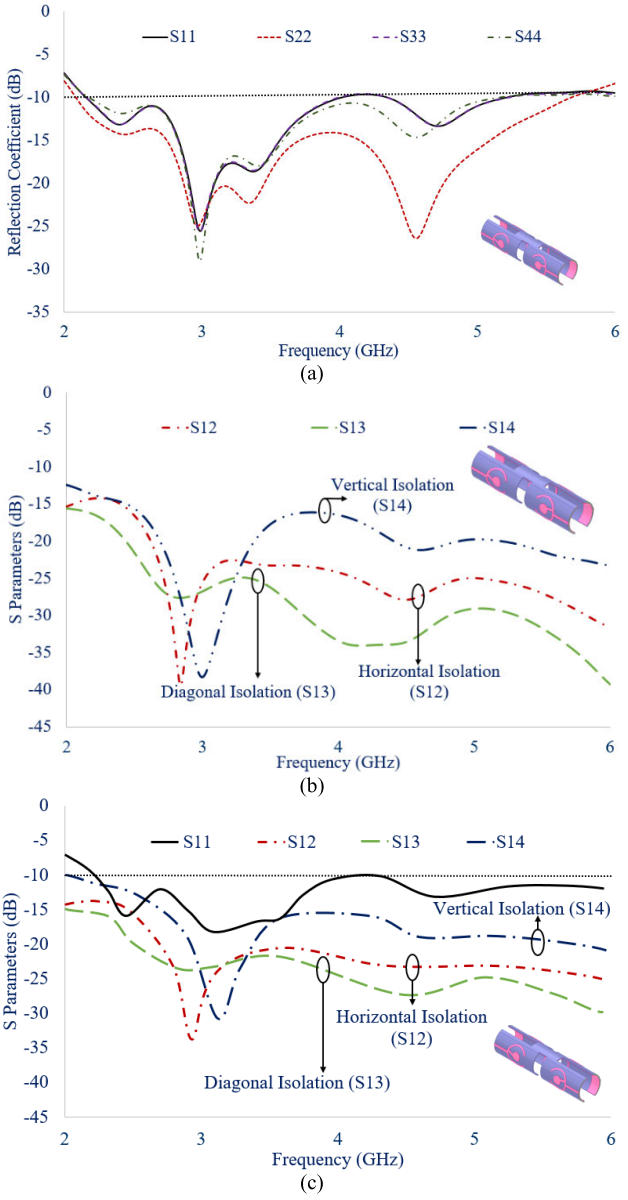

FIGURE 19. Measured S-parameters of 4 elements flexible MIMO antenna for bending along X-Axis (a) Scattering parameters (b) Transmission parameters (c) Measured S-parameters.

IV. BENDING ANALYSIS

To figure out the effect of the flexible operation of the proposed transparent MIMO antenna on RF performance parameters is important for the reliable operation on the conformal surfaces. Due to the variation of resonant electrical length in the bent MIMO antenna, the performance parameters have to be checked through the bending analysis. The simulated and fabricated bending scenarios are presented in Fig. 17 where a semi-cylindrical Styrofoam ($\varepsilon_r = 1.03$) is utilized to position the transparent MIMO antenna with the prescribed bending angle. The antenna performance validation for the flexible operation conditions is carried out by plotting ECC and scattering parameters by exciting Port 1 where the antenna is bent to 300° along the X-axis and Y-axis. The case of a 300° bending angle is selected as the worst-case scenario after checking the maximum bending capability of the antenna.

Fig. 18 (a-c) and Fig. 19 (a-c) show the simulated and measured scattering parameters under the 300° bending angle configuration. Almost identical impedance bandwidth from 2.22 GHz to 6 GHz along X-axis bending and from 2.16 GHz to 4.01 GHz and from 4.35 GHz to 5.2 GHz in two separate bands along Y-axis is observed, that agrees well with the numerical computation results. In both cases, the port isolation levels are greater than 15dB thus satisfying the isolation criteria for MIMO antenna performance.

The co/cross-polarization far-field patterns for 4 elements MIMO antenna by bending the antenna at 300° along the

TABLE 1. Comparison of proposed transparent structure with wide-band 4-element MIMO antennas from literature.

Reference	AT	Thickness	IBW	RE (%)	Sheet Impedance (Ω/Sq)	I (dB)	ECC	T	RP	CG	Flexible	Material
22	40×40 (2 element)	1.124mm	2.4-2.48, 5.15-5.8	43% (2.44 GHz) 46% (5.5 GHz)	0.05	>15	--	Yes	O	Yes	Yes	MMMC (micro-metal mesh conductive) film and glued on a glass substrate
23	22x31 (2 element)	0.125mm	3.43-10.1	63	Very low	>15	<0.3	No	B	Yes	Yes	conductive silver nanoparticles ink Kapton (Substrate)
24	126x70 (2 element)	4.27mm	9.13% (5.8 GHz center)	72	Very low	>30	0.001	No	D	Yes	Yes	Conductive copper foil flexible multilayered polydimethylsiloxane (PDMS) substrate
25	38.1x38.1 (2 element)	2mm	20% (2.4-2.5 GHz)	27	Very low	>12	<0.01	No	O	Yes	Yes	Conductive copper Felt substrate
26	180x180 (4 element)	1.52mm	0.7-1.01 2.6-3.18 5.3-6.06 6.7-6.94	70	Very low	~10 (<1 GHz) ~13 (>2.6 GHz band)	<0.5	No	D and B	Yes	Yes	Thick flexible Rogers RO3003
27	31.62 x 3.3 (single element) (8 cell series forming an array with intermediate feeding) repeated 4 times	0.5mm	11.6% (35 GHz Centre)	--	Very low	>40	--	No	--	--	Yes	RT/duroid5880
28	11x25.4 (2 element)	0.147mm	27.2-40	--	0.00028	>20	<0.06	No	B	Yes	Yes	Silver nanoparticle ink PET film
29	60×60 (4 element)	0.2mm	4.4-5	85%	0.0025	>20	<0.005	Yes	O	Yes	Yes	Ni-based embedded metallic mesh (EMM) PET
Prop	**66x45 (4 element)**	**0.625mm**	**2.21-6**	**~41%**	**4**	**>15**	**<0.016**	**Yes**	**D and B**	**Yes**	**Yes**	AgHT-4 Malinex (ST507)

[A_t: Total Area (at the lowest operating frequency), CG: Common Ground, ECC: Envelope Correlation Coefficient, IBW: Impedance Bandwidth, I: Isolation, RE: Radiation Efficiency, RP: Radiation Pattern (O: Omnidirectional, D: Directional, B: Bidirectional), T: Transparent,].

X- and Y-axis are shown in Fig. 20 (a-b). It can be observed that by bending the antenna along the X- and Y-axis the E-plane pattern is affected, where instead of a dipole-shaped pattern achieved for unbend condition, an omnidirectional pattern with a slight tilt is achieved. Due to the bending of the antenna, the cross-pol levels have degraded as compared to the antenna under unbent conditions however the levels are still more than 10 dB.

Fig 21 (a-b) illustrates that ECC value is well below 0.1 in the first band between 2.2 GHz and 3.81 GHz, and in the second band between 4.24 GHz and 6 GHz whereas an ECC value greater than 0.1 is observed between 3.81 GHz and 4.24 GHz due to the degradation in the isolation level, S21 through the bending along Y-axis.

In the case of bending along the X-axis, ECC $>$ 0.1 is also observed at the lower band between 2.79 GHz and

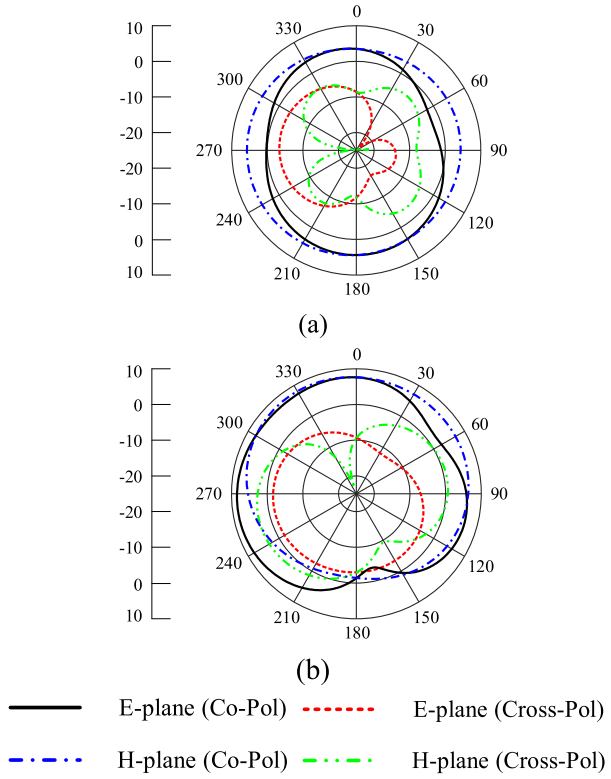

FIGURE 20. 2D Co/Cross Pol Radiation pattern at 3 GHz for 4 element antennas by bending the antenna at 300° along (a) X-axis (b) Y-axis.

3.03 GHz as observed in Fig. 21 (c) whereas the satisfactory ECC value is less than 0.1 is achieved for the rest of the operating frequency band. The ECC 12 is measured by bending the antenna along the X and Y axis as shown in Fig 21 (b and d) where it is observed that the numerically computed and experimentally measured results of ECC 12 agree well due to which the other MIMO system parameters including measured ECC 13 and ECC 14 are not shown for the brevity of data.

The higher ECC value in maximum bending condition along X and Y axes in comparison to ECC value in no bending condition can be attributed to the improved closer proximity of individual antenna elements, which degrades the port isolation level among antenna elements. The symmetrical geometrical positioning of antenna elements is also deteriorated, which can be deduced from the differences in the reflection parameters of each antenna element.

It is observed from Fig. 22 that maximum gain and average efficiency when the antenna is bent along X-axis are 0.47 dBi and 34% whereas for Y-axis bending the maximum gain and average efficiency are 1.07 dBi and 33%, respectively.

Table 1 shows a detailed performance comparison table among some notable MIMO antenna designs in the literature. Since these antennas are designed with different geometrical structures, the type of radiation pattern is also added to the table. As deduced from Table 1, the proposed system achieves a reasonable performance while ensuring a connected ground plane for practical application [24].

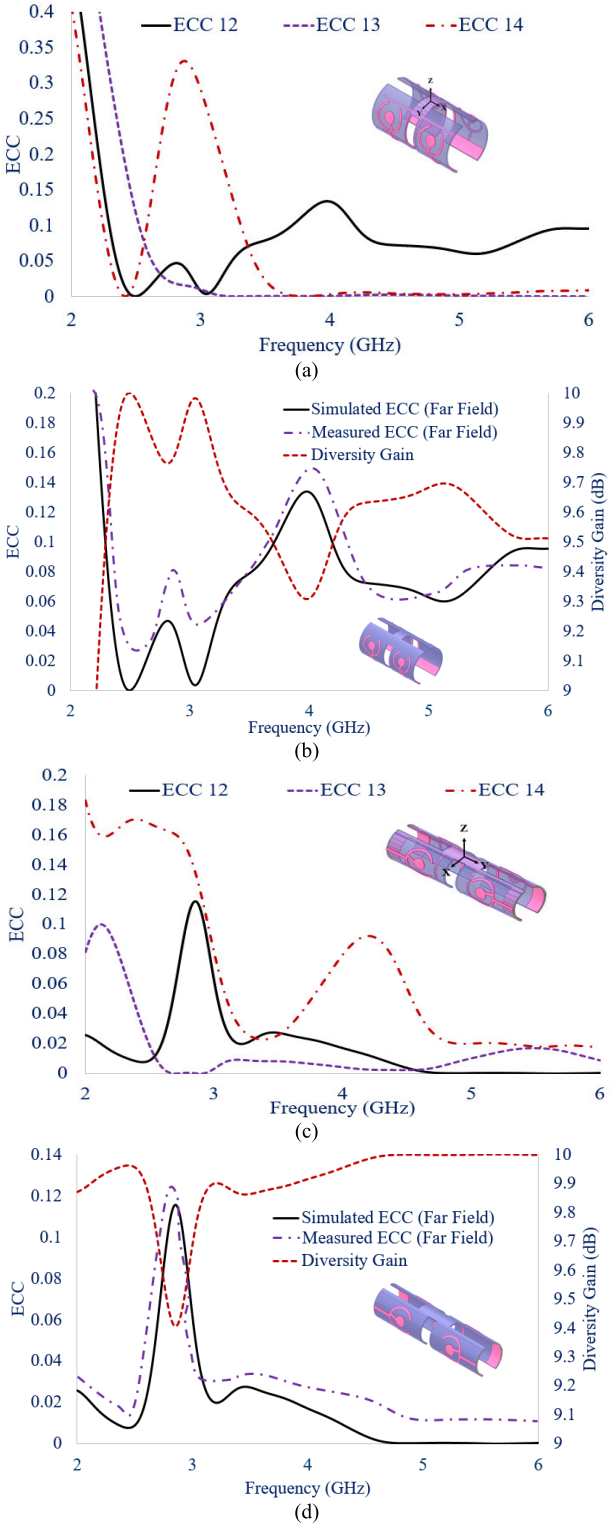

FIGURE 21. (a) Simulated Frequency-variation of Envelope Correlation Coefficient (ECC) by Bending along Y-Axis (b) ECC and Diversity Gain (DG) by Bending along Y-Axis (c) Simulated Frequency-variation of: Envelope Correlation Coefficient (ECC) by Bending along X-Axis (d) ECC and Diversity Gain (DG) by Bending along X-Axis.

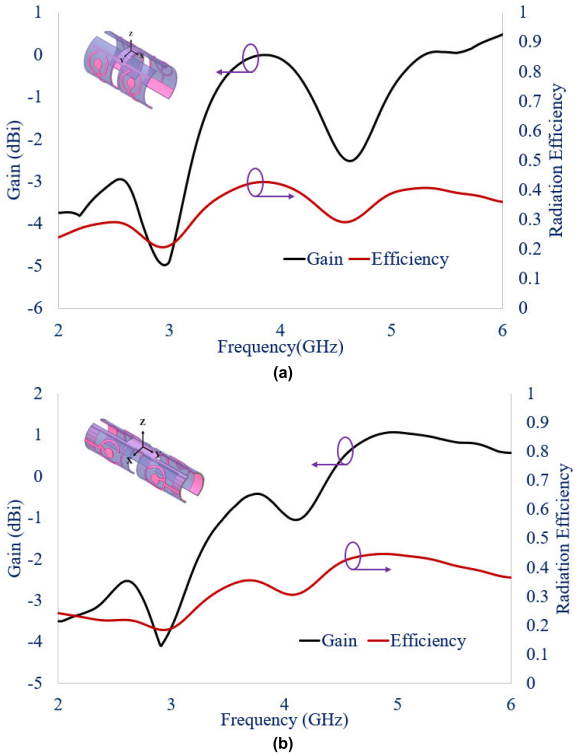

FIGURE 22. Gain and Efficiency plot for 4 element antennas by bending along (a) Y-axis (b) X-axis.

V. CONCLUSION

In this paper, we focus on providing an alternative solution for the connected ground plane in a flexible transparent MIMO planar monopole antenna. Under the critical manufacturing constraints of a transparent antenna structure, the design of these connected lines is crucial for the overall antenna performance. The final design demonstrates an impedance bandwidth of 3.79 GHz with a percentage bandwidth of 92.32% between 2.21 GHz and 6 GHz with an inter-element isolation level greater than 15dB. The maximum gain is 0.53dBi with the minimum efficiency of 41%, respectively, which is satisfactory considering flexible structure and sheet impedance of 4 Ω/sq.

The proposed flexible optically transparent antenna can be useful for indoor smart wireless devices like routers and repeaters working in the Sub-6 GHz 5G band which can be interfaced on the glass windows of the home and office buildings thus maintaining the aesthetics by being visibly neutral. In addition, such transparent antennas in the form of arrays can be used in the satellites having small form factor, and cube satellites that help meeting the critical space requirements [34], [35]. Thin film transparent antennas can be easily integrated over the solar panels thus no extra space needs to be reserved within the chassis while it helps in the generation of revenue by leasing the panels to the telecom companies [34]–[36].

REFERENCES

[1] A. Nordrum and K. Clark. (Jan. 2017). *IEEE Spectrum: Everything You Need to Know About 5G*. [Online]. Available: https://spectrum.ieee.org/video/telecom/wireless/everything-you-need-to-know-about-5g

[2] W. Hong, S. Lim, S. Ko, and Y. G. Kim, "Optically invisible antenna integrated within an OLED touch display panel for IoT applications," *IEEE Trans. Antennas Propag.*, vol. 65, no. 7, pp. 3750–3755, Jul. 2017.

[3] E. H. Lim, K. W. Leung, X. Fang, and Y. Pan, *Transparent Antennas: Wiley Encyclopedia of Electrical and Electronics Engineering*. New York, NY, USA: Wiley, 2015, pp. 1–23.

[4] T. Peter, R. Nilavalan, H. F. A. Tarboush, and S. W. Cheung, "A novel technique and soldering method to improve performance of transparent polymer antennas," *IEEE Trans. Antennas Propag. Lett.*, vol. 9, pp. 918–921, 2010.

[5] D. W. Bliss, K. W. Forsythe, and A. M. Chan, "MIMO wireless communication," *Lincoln Lab. J.*, vol. 15, pp. 97–126, 2005.

[6] M. A. Jensen and J. W. Wallace, "A review of antennas and propagation for MIMO wireless communications," *IEEE Trans. Antennas Propag.*, vol. 52, no. 11, pp. 2810–2824, Nov. 2004.

[7] S.-C. Chen, L.-C. Chou, C.-I.-G. Hsu, and S.-M. Li, "Compact sub-6-GHz four-element MIMO slot antenna system for 5G tablet devices," *IEEE Access*, vol. 8, pp. 154652–154662, 2020.

[8] J. Y. Deng, J. Li, L. Zhao, and L. Guo, "A dual-band inverted-F MIMO antenna with enhanced isolation for WLAN applications," *IEEE Antennas Wireless Propag. Lett.*, vol. 16, pp. 2270–2273, 2017.

[9] A. MoradiKordalivand, T. A. Rahman, and M. Khalily, "Common elements wideband MIMO antenna system for WiFi/LTE access-point applications," *IEEE Antennas Wireless Propag. Lett.*, vol. 13, pp. 1601–1604, 2014.

[10] D. Sarkar and K. V. Srivastava, "A compact four-element MIMO/diversity antenna with enhanced bandwidth," *IEEE Antennas Wireless Propag. Lett.*, vol. 16, pp. 2469–2472, 2017.

[11] D. Sarkar and K. V. Srivastava, "Compact four-element SRR-loaded dual-band MIMO antenna for WLAN/WiMAX/WiFi/4G-LTE and 5G applications," *Electron. Lett.*, vol. 53, no. 25, pp. 1623–1624, Dec. 2017.

[12] S. Saxena, B. K. Kanaujia, S. Dwari, S. Kumar, and R. Tiwari, "MIMO antenna with built-in circular shaped isolator for sub-6 GHz 5G applications," *Electron. Lett.*, vol. 54, no. 8, pp. 478–480, Apr. 2018.

[13] H. Wang, L. Liu, Z. Zhang, Y. Li, and Z. Feng, "A wideband compact WLAN/WiMAX MIMO antenna based on dipole with V-shaped ground branch," *IEEE Trans. Antennas Propag.*, vol. 63, no. 5, pp. 2290–2295, May 2015.

[14] H. Li, J. Xiong, and S. He, "A compact planar MIMO antenna system of four elements with similar radiation characteristics and isolation structure," *IEEE Antennas Wireless Propag. Lett.*, vol. 8, pp. 1107–1110, 2009.

[15] M. S. Sharawi, "Current misuses and future prospects for printed multiple-input, multiple-output antenna systems," *IEEE Antenna Propag Mag.*, vol. 59, no. 2, pp. 162–170, Apr. 2017.

[16] T. Alam, S. R. Thummaluru, and R. K. Chaudhary, "Integration of MIMO and cognitive radio for sub-6 GHz 5G applications," *IEEE Antennas Wireless Propag. Lett.*, vol. 18, no. 10, pp. 2021–2025, Oct. 2019.

[17] R. Anitha, P. V. Vinesh, K. C. Prakash, P. Mohanan, and K. Vasudevan, "A compact quad element slotted ground wideband antenna for MIMO applications," *IEEE Trans. Antennas Propag.*, vol. 64, no. 10, pp. 4550–4553, Oct. 2016.

[18] A. Desai, T. Upadhyaya, M. Palandoken, and C. Gocen, "Dual band transparent antenna for wireless MIMO system applications," *Microw. Opt. Technol. Lett.*, vol. 61, no. 7, pp. 1845–1856, Jul. 2019.

[19] Q. L. Li, S. W. Cheung, D. Wu, and T. I. Yuk, "Optically transparent dual-band MIMO antenna using micro-metal mesh conductive film for WLAN system," *IEEE Antennas Wireless Propag. Lett.*, vol. 16, pp. 920–923, 2016.

[20] K. K. So, B. J. Chen, C. H. Chan, and K. M. Luk, "Study of MIMO antenna made of transparent conductive ITO films," in *Proc. IEEE Asia–Pacific Microw. Conf. (APMC)*, Singapore, Dec. 2019, pp. 515–517.

[21] A. Desai, C. D. Bui, J. Patel, T. Upadhyaya, G. Byun, and T. K. Nguyen, "Compact wideband four element optically transparent MIMO antenna for mm-wave 5G applications," *IEEE Access*, vol. 8, pp. 194206–194217, 2020.

[22] Q. L. Li, S. W. Cheung, D. Wu, and T. I. Yuk, "Optically transparent dual-band MIMO antenna using micro-metal mesh conductive film for WLAN system," *IEEE Antennas Wireless Propag. Lett.*, vol. 16, pp. 920–923, 2017.

[23] W. Li, Y. Hei, P. M. Grubb, X. Shi, and R. T. Chen, "Compact inkjet-printed flexible MIMO antenna for UWB applications," *IEEE Access*, vol. 6, pp. 50290–50298, 2018.

[24] A. S. M. Alqadami, M. F. Jamlos, P. J. Soh, and G. A. Vandenbosch, "Assessment of PDMS technology in a MIMO antenna array," *IEEE Antennas Wireless Propag. Lett.*, vol. 15, pp. 1939–1942, 2016.

[25] H. Li, S. Sun, B. Wang, and F. Wu, "Design of compact single-layer textile MIMO antenna for wearable applications," *IEEE Trans. Antennas Propag.*, vol. 66, no. 6, pp. 3136–3141, Jun. 2018.
[26] K. R. Jha, Z. A. P. Jibran, C. Singh, and S. K. Sharma, "4-port MIMO antenna using common radiator on a flexible substrate for sub-1 GHz, sub-6 GHz 5G NR, and Wi-Fi 6 applications," *IEEE Open J. Antennas Propag.*, vol. 2, pp. 689–701, 2021.
[27] Q. Wang, N. Mu, L. Wang, S. Safavi-Naeini, and J. Liu, "5G MIMO conformal microstrip antenna design," *Wireless Commun. Mobile Comput.*, vol. 2017, Dec. 2017, Art. no. 7616825.
[28] S. F. Jilani, A. Rahimian, Y. Alfadhl, and A. Alomainy, "Low-profile flexible frequency-reconfigurable millimetre-wave antenna for 5G applications," *Flexible Printed Electron.*, vol. 3, no. 3, 2018, Art. no. 035003.
[29] H. Qiu, H. Liu, X. Jia, Z.-Y. Jiang, Y.-H. Liu, J. Xu, T. Lu, M. Shao, T.-L. Ren, and K. J. Chen, "Compact, flexible, and transparent antennas based on embedded metallic mesh for wearable devices in 5G wireless network," *IEEE Trans. Antennas Propag.*, vol. 69, no. 4, pp. 1864–1873, Apr. 2021.
[30] M. A. Abdalla and A. A. Ibrahim, "Compact and closely spaced metamaterial MIMO antenna with high isolation for wireless applications," *IEEE Antennas Wireless Propag. Lett.*, vol. 12, pp. 1452–1455, 2013.
[31] M. S. Sharawi, "Printed multi-band MIMO antenna systems and their performance metrics," *IEEE Antennas Propag. Mag.*, vol. 55, no. 5, pp. 218–232, Oct. 2013.
[32] A. I. Najam, Y. Duroc, and S. Tedjini, "Multiple-input multiple output antennas for ultra-wideband communications," *Intech Open*, vol. 10, pp. 209–236, Oct. 2012.
[33] S. A. Saputro, S. Nandiwardhana, and J.-Y. Chung, "Estimation of antenna correlation coefficient of n-port lossy MIMO array," *ETRI J.*, vol. 40, no. 3, pp. 303–308, Jun. 2018.
[34] C. White and H. R. Khaleel, "Flexible optically transparent antennas," in *WIT Transactions on State of the Art in Science and Engineering*, vol. 82. WIT Press, 2014, p. 59, doi: 10.2495/978-1-84564-986-9/003.
[35] X. Liu, D. R. Jackson, J. Chen, J. Liu, P. W. Fink, G. Y. Lin, and N. Neveu, "Transparent and nontransparent microstrip antennas on a CubeSat: Novel low-profile antennas for CubeSats improve mission reliability," *IEEE Antennas Propag. Mag.*, vol. 59, no. 2, pp. 59–68, Apr. 2017.
[36] M. J. Roo-Ons, S. V. Shynu, M. J. Ammann, S. J. McCormack, and B. Norton, "Transparent patch antenna on a-Si thin-film glass solar module," *Electron. Lett.*, vol. 47, no. 2, pp. 85–86, 2011.

ARPAN DESAI (Senior Member, IEEE) received the B.E. degree in electronics and communication engineering from Sardar Patel University, Gujarat, India, in 2006, the M.Sc. degree in wireless communication systems from Brunel University London, London, U.K., in 2008, and the Ph.D. degree in the field of transparent antennas from the Charotar University of Science and Technology, Gujarat, in January 2020. He is currently working as a Postdoctoral Researcher with Ton Duc Thang University, Ho Chi Minh City, Vietnam. He is also working as an Assistant Professor with the Department of Electronics and Communication Engineering, Charotar University of Science and Technology. He has published more than 45 research articles, mostly in SCI/ Scopus journals, international conferences, and book chapters. His current research interests include transparent antennas for MIMO applications, energy harvesting devices, transparent DRAs, flexible wearable antennas, transparent antennas, and MIMO antennas. He is serving as the Technical Activity Chair for the IEEE Signal Processing Society, Gujarat Section, India. He is an Associate Editor of the journal *Wireless Power Transfer*, Cambridge University Press.

MERIH PALANDOKEN (Senior Member, IEEE) received the M.S. degree in microelectronics and microsystems engineering from the Hamburg University of Technology, Hamburg, Germany, in 2005, under DAAD Scholarship, and the Ph.D. degree in theoretical electrical engineering from the Technical University of Berlin, Germany, in 2012. He is currently working with the Department of Electrical and Electronics Engineering, Izmir Katip Celebi University, as the Vice Head of the Department. He is also working as the Vice Head of the Artificial Intelligence and Data Science Research and Application Center and the Smart Factory Systems Research and Application Center, Izmir Katip Celebi University. His research interests include analytical/numerical design and modeling of active/passive wireless components in the micro/millimeter wave frequencies, especially in the field of RF energy harvesting systems, compact microwave absorbers, machine learning-based smart RF component and the IoT compatible sensor design, microwave probe design, electrically small bioimplantable antennas, and RFID systems.

JAYSHRI KULKARNI (Member, IEEE) received the B.E. degree in electronics and telecommunication engineering from Shivaji University, Maharashtra, India, in 2005, the M.E. degree in microwave engineering from PICT College, Pune, Maharashtra, in 2011, and the Ph.D. degree in electronics and communication engineering from Anna University, Chennai, India, in 2020. From 2006 to 2009, she was a Lecturer with the Genba Sopanrao Moze College of Engineering, Pune. Since 2010, she has been working as an Assistant Professor with the Department of Electronics and Telecommunication Engineering, Vishwakarma Institute of Information Technology, Pune, India. She has authored more than ten books and more than 25 research articles. Her research interests include antennas, microwave engineering, wireless communication, and wireless sensor networks. She served as a TPC Member for WCI 2018/2019 and of SSCC 2019. She has also worked as an Advisory Committee Member at I7C-2019.

GANGIL BYUN (Senior Member, IEEE) received the B.S. and M.S. degrees in electronic and electrical engineering from Hongik University, Seoul, South Korea, in 2010 and 2012, respectively, and the Ph.D. degree in electronics and computer engineering from Hanyang University, Seoul, in 2015. After his graduation, he returned to Hongik University to work as a Research Professor and performed active research for two years. He joined the Faculty of Ulsan National Institute of Science and Technology (UNIST), in February 2018, where he is currently an Assistant Professor of electrical engineering. His principal areas of research include the design and analysis of small antenna arrays for adaptive beamforming applications, such as direction of arrival estimation, interference mitigation, and radar. His recent research interests also include display-integrated antennas, optically-invisible antennas, and wireless backhaul antennas for 5G communications. He has actively contributed to the consideration of both antenna characteristics and signal processing perspectives for the improvement of overall beamforming performances.

TRUONG KHANG NGUYEN (Member, IEEE) received the B.S. degree in computational physics from the University of Science, Vietnam National University, Ho Chi Minh City, Vietnam, in 2006, and the M.S. and Ph.D. degrees in electrical and computer engineering from Ajou University, Suwon, South Korea, in 2013. From October 2013 to December 2014, he worked at the Division of Energy Systems Research, Ajou University, as a Postdoctoral Fellow. He is currently an Assistant Director, and also the Head of the Division of Computational Physics, Institute for Computational Science, Ton Duc Thang University, Ho Chi Minh City. His current research interests include microwave antennas for wireless communication, terahertz antennas for compact and efficient sources, nanostructures and nanoantennas for optical applications, and computational micro/nano structures.